

Superstatistical approach to air pollution statistics

Griffin Williams,¹ Benjamin Schäfer,^{1,*} and Christian Beck^{1,†}

¹*School of Mathematical Sciences, Queen Mary University of London, London E1 4NS, United Kingdom*

Air pollution by Nitrogen Oxides (NO_x) is a major concern in large cities as it has severe adverse health effects. However, the statistical properties of air pollutants are not fully understood. Here, we use methods borrowed from nonequilibrium statistical mechanics to construct suitable superstatistical models for air pollution statistics. In particular, we analyze time series of Nitric Oxide (*NO*) and Nitrogen Dioxide (*NO*₂) concentrations recorded at several locations throughout Greater London. We find that the probability distributions of concentrations have heavy tails and that the dynamics is well-described by χ^2 superstatistics for *NO* and inverse χ^2 superstatistics for *NO*₂. Our results can be used to give precise risk estimates of high-pollution situations and pave the way to mitigation strategies.

Complex driven non-equilibrium systems with time scale separation are often well-described by superstatistical methods, i.e. by mixing several dynamics on distinct time scales and constructing effective statistical mechanics models out of this mixing [1, 2]. The intensive parameter β that fluctuates in a superstatistical way can be an inverse temperature of the system, a fluctuating diffusion constant, or simply a local variance parameter in a given time series generated by the complex system under consideration. This formalism is in particular relevant for heterogenous spatio-temporally varying systems and has been successfully applied to many areas of physics and beyond, most notably Lagrangian turbulence [3], defect turbulence [4], wind velocity fluctuations [5], share price dynamics [6], diffusion of complex bio-molecules [7], frequency fluctuations in power grids [8], rainfall statistics [9, 10], and many more. In this Letter, we apply a superstatistical analysis to an important topic of high relevance, namely the spatio-temporally dynamics of air pollution in big cities. Our main example of pollutants considered in the following are *NO* and *NO*₂, but the method can be similarly applied to other substances.

NO and *NO*₂ are examples of nitrogen oxides (*NO*_x), which are gaseous air pollutants that are primarily discharged through combustion [11]. In urban areas, the main cause of this is through automobile emissions [12]. These chemicals have been shown to aggravate asthma and other respiratory symptoms and increase mortality. Further, short term exposure to *NO*₂ has been shown to correlate with ischaemic and hemorrhagic strokes [11, 13, 14]. While *NO* is a very important substance with Earth's ecosystem, for example regulating the development in plants and acting as a signaling hormone in certain processes in animals, it can also cause severe environmental damage in high concentrations [15–17]. *NO* may form acids, e.g. by chemically mixing with water (*H*₂*O*) to form Nitric Acid (*HNO*₃), or reacting further to *NO*₂ [18] it can cause acid rain [14]. Though *NO*_x are not thought to be carcinogenic, they indicate the presence of other harmful air pollutants [12].

The data analyzed in this Letter was taken from the publicly available London Air Quality Network (LAQN)

website [19]. The site provides readings of pollutant levels at different locations throughout Greater London at different time intervals, with the 15-minute interval data analyzed here. Inspecting the measured concentration time series for both *NO* and *NO*₂ reveals that both pollutants' concentrations vary on multiple time scales, see Fig. 1.

Concentrating on the case of *NO* for now, we notice that the probability distribution of the measured concentration exhibits power law tails, see Fig. 2. The distribution is well-fitted by a *q*-exponential [20] of the form

$$p(u) = (2 - q)\lambda_q [1 + (q - 1)\lambda_q u]^{-\frac{1}{1-q}}, \quad (1)$$

where *u* are the concentration levels [$\mu\text{g}/\text{m}^3$] of the pollutant, and the *q*- and λ_q -values are parameters. *q* can be regarded as an entropic index [20–22] and it is related to λ_q and the mean μ by

$$\lambda_q = \frac{1}{\mu(3 - 2q)}, \quad (2)$$

see supplementary material (SM) for more details.

The basic idea of the superstatistical modelling approach is that a given time series, generated by a complex driven nonequilibrium systems, obeys a stochastic differential equation (SDE) where the parameters of the SDE change randomly as well, but on a much longer time scale [23]. In our case, the concentration time series, whilst being *q*-exponentially distributed as a whole, appears to be non-stationary, in the sense that it can be divided into shorter time slices, of length *T*, that each have locally an exponential density with different relaxation constants λ_e each, see Fig. 3. These changes in the pollutants statistics make sense due to the changing environment, e.g. because of changing weather conditions or traffic flow varying from week to week and also across seasons. Observing simple (exponential) statistics locally, while noting heavy tails in the aggregated statistics clearly suggests a superstatistical description. One of the simplest local models is based on an exponential probability distribution of the form

$$p(u|\beta) = \beta \cdot \exp(-\beta u), \quad (3)$$

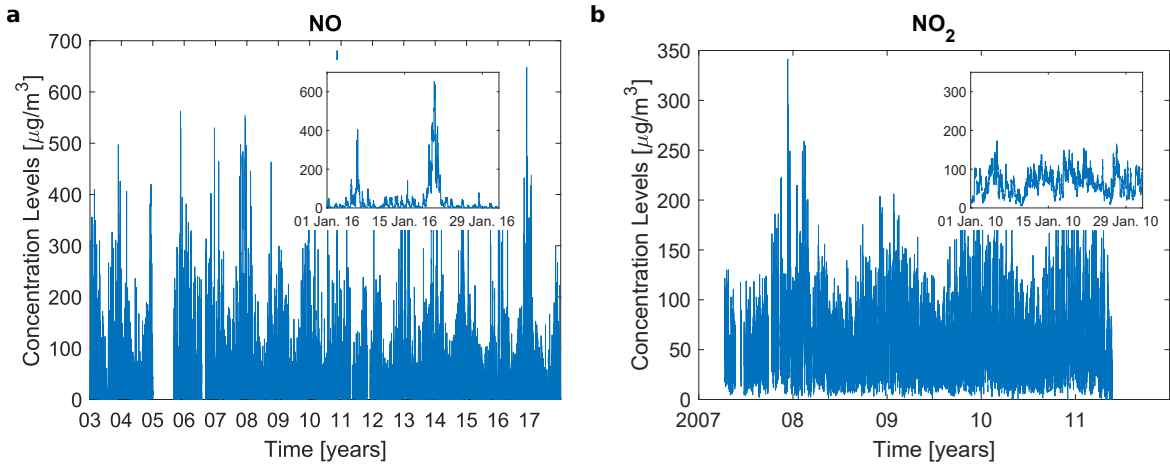


Figure 1. The concentration levels vary on several distinct time scales. a: We display the concentration of NO , recorded at the Sir John Cass School location (London), measured in 15-minute intervals. The inset reveals large variations within one month. b: We plot the concentration of NO_2 , recorded at the North Street location (London), measured in 15-minute intervals. The inset again gives the concentrations for one month. For both pollutants we note seasonal changes, weekly changes and intermittent fluctuations.

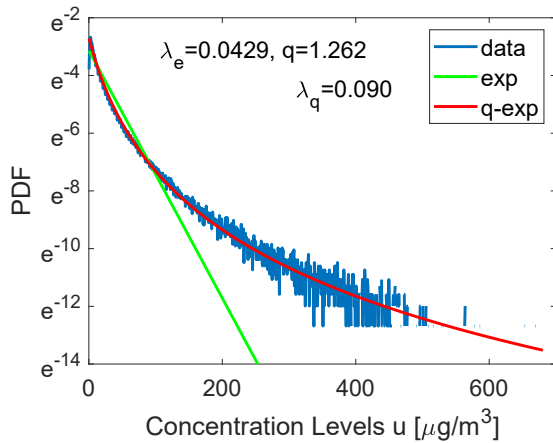


Figure 2. Pollution statistics is not exponentially distributed, but rather q -exponentially distributed. We display the histogram of the NO data, together with the best exponential fit (green) and a q -exponential fit (red). Also displayed are the value of the exponential parameter λ_e and the q - and λ_q -parameters for the q -exponential distribution.

where $\beta = \lambda_e$ is a local relaxation parameter that fluctuates on the larger superstatistical time scale.

We determine this large time scale by computing the average local kurtosis κ of a cell of length Δt , similarly as done in [2] for locally Gaussian distributions. We use a local average kurtosis defined as

$$\kappa(\Delta t) = \frac{1}{t_{max} - \Delta t} \int_0^{t_{max} - \Delta t} dt_0 \frac{\langle (u - \bar{u})^4 \rangle_{t_0, \Delta t}}{\langle (u - \bar{u})^2 \rangle_{t_0, \Delta t}^2}, \quad (4)$$

where t_{max} is the full length of the time series. The notation $\langle \dots \rangle_{t_0, \Delta t}$ indicates the expectation for the time

slice of length Δt starting at t_0 . Assuming local exponential distributions with kurtosis 9, we apply Equation (4) to determine the long time scale T as the special time length Δt such that

$$\kappa(\Delta t) = \kappa(T) = 9. \quad (5)$$

We show an example of how T is calculated in the SM, with a plot illustrating how the average local kurtosis depends on Δt . Once the time slice length T is calculated, we define an intensive parameter β for each local cell, by setting $\beta = \lambda_e = 1/\langle u \rangle_{t_0, T}$. The distribution of this parameter, $f(\beta)$, is then obtained from a histogram, as shown in Fig. 4a. In good approximation, we find β to be χ^2 distributed, i.e.,

$$f(\beta) = \frac{1}{\Gamma(\frac{n}{2})} \left(\frac{n}{2\beta_0} \right)^{\frac{n}{2}} \beta^{\frac{n}{2}-1} \exp\left(-\frac{n\beta}{2\beta_0}\right), \quad (6)$$

where n is the number degrees of freedom and β_0 is the mean of β .

Integrating out the β -parameter, the marginal distribution $p(u)$ is calculated as

$$p(u) = \int_0^\infty p(u|\beta) f(\beta) d\beta, \quad (7)$$

which evaluates to

$$p(u) = (2-q)\lambda_q [1 + (q-1)\lambda_q u]^{\frac{1}{1-q}}, \quad (8)$$

with

$$-\frac{n}{2} - 1 = \frac{1}{1-q}, \quad (9)$$

and

$$\frac{1}{2}(q-1)\lambda_q = \frac{\beta_0}{n}. \quad (10)$$

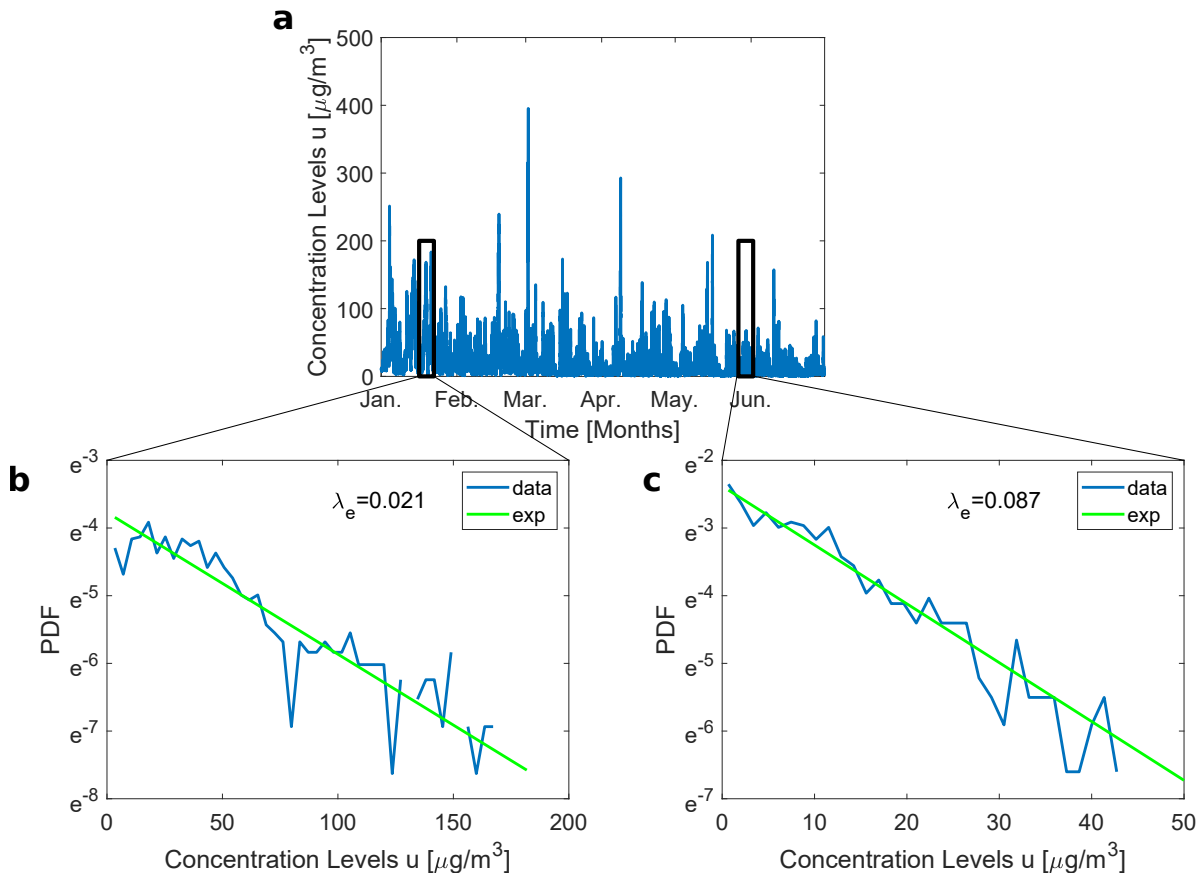


Figure 3. *NO* concentrations locally follow exponential distributions. a: We plot the *NO* concentration for several months in 2010, with two periods of length $\Delta t = T \approx 6$ days highlighted, whose distributions are explored in panels b and c. The histograms of panels b and c are fitted with exponential distributions and we note their respective λ_e -values. Note that the exponent in panel b is only one fourth of the exponent recovered in panel c, i.e. high pollution levels are much more likely to be observed in panel b, a time period in January, than in panel c, a time period in June. These different exponents quantify the observation that pollutant levels tend to be higher during winter than during summer, see also Fig. 1.

Eq. (8) is the q -exponential distribution, which we derived from a superposition of local exponential distributions.

Fitting the n -parameter to find $f(\beta)$, as illustrated in Fig. 4a, we determine the q - and λ_q -parameters from Eqs. (9) and (10), respectively. Using the χ^2 -distribution $f(\beta)$, we use (7) and (8) to compute a probability density which both approximates the fitted q -exponential and the data very well, successfully serving as a consistency check of the superstatistical approach, see Fig. 4b.

We already noticed different statistical behavior when inspecting the trajectory of the *NO*₂ data in Fig. 1, as compared to that of *NO*. Following a similar procedure as for the *NO* data, we find that for *NO*₂ the aggregated distribution is approximated by a q -Maxwell Boltzmann distribution, of the form

$$p(u) = \frac{1}{Z} u^2 \sigma_q^{3/2} [1 + (q-1)\sigma_q u^2]^{-\frac{1}{q-1}}, \quad (11)$$

where Z is the normalization factor given by

$$Z = \frac{\sqrt{\pi} \Gamma\left(\frac{5-3q}{2(q-1)}\right)}{4(q-1)^{3/2} \Gamma\left(\frac{1}{q-1}\right)} \quad (12)$$

and where q is related to the scale parameter σ_q and the mean μ by

$$\sigma_q = \left(\frac{2(q-1)^{3/2} \Gamma\left(\frac{1}{q-1}\right)}{\mu \sqrt{\pi} (2-q) (3-2q) \Gamma\left(\frac{5-3q}{2(q-1)}\right)} \right)^2, \quad (13)$$

see SM for details.

Analogously to the *NO*-case, we explain the aggregated distribution as a superposition of simple local distributions, here chosen as ordinary Maxwell-Boltzmann distributions. Each local Maxwell-Boltzmann distribution is defined as

$$p(u) = \sqrt{\frac{16}{\pi}} u^2 \sigma_{mb}^{3/2} \exp(-\sigma_{mb} u^2), \quad (14)$$

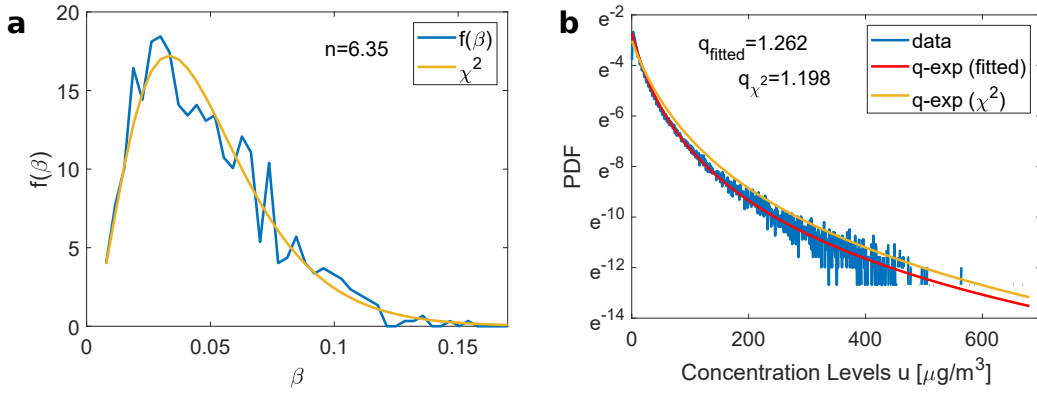


Figure 4. The superstatistical approach consistently describes the data. a: The distribution of local exponents of the NO data, here named β , follows a χ^2 distribution, one of three commonly observed universality classes in general superstatistical complex systems [2]. b: Histogram of the NO data, together with a q -exponential distribution with fitted q - and λ_q -values (red), and a q -exponential distribution with q - and λ_q -values derived from the parameters of the fitted χ^2 -distributed $f(\beta)$ (orange).

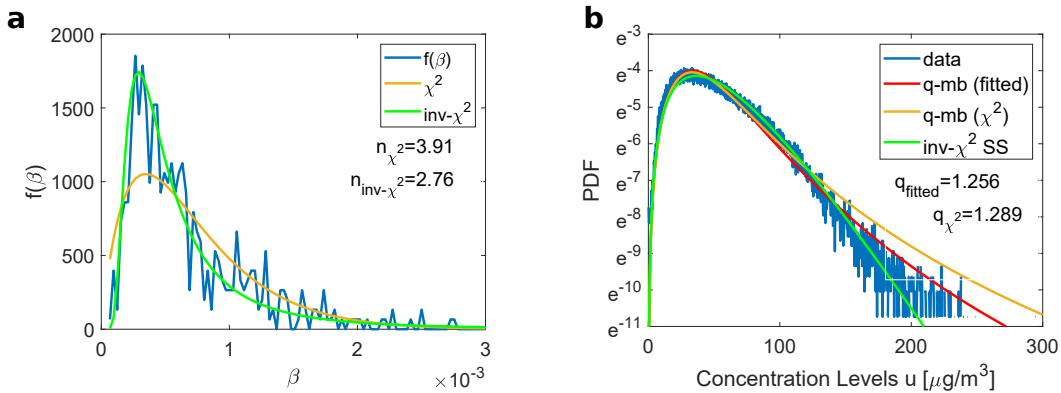


Figure 5. NO_2 concentrations are well described by inverse χ^2 superstatistics. a: The extracted distribution of the scale parameter β for the NO_2 time series is very well fitted by an inverse- χ^2 distribution (green). b: Histogram of the NO_2 data, together with a q -Maxwell-Boltzmann distribution with fitted q - and σ_q -values (red) and a q -Maxwell-Boltzmann with q - and σ_q -values superstatistically calculated from a χ^2 distributed $f(\beta)$ (orange), and Eq. (17), which is calculated from inverse- χ^2 superstatistics (green). The inverse χ^2 superstatistics fits the NO_2 data best.

where $\sigma_{mb} = \beta$ is a scale parameter.

We determine the long time scale T by varying Δt so that we locally obtain the kurtosis of a Maxwell-Boltzmann distribution, which is given as

$$\kappa(T) = \frac{15\pi^2 + 16\pi - 192}{(3\pi - 8)^2} \approx 3.1082, \quad (15)$$

see SM for the calculation.

The results of our superstatistical analysis for the NO_2 data are displayed in Fig. 5. We find that the histogram of β is best fitted by an inverse- χ^2 distribution

$$f(\beta) = \frac{\beta_0}{\Gamma(\frac{n}{2})} \left(\frac{n\beta_0}{2}\right)^{\frac{n}{2}} \beta^{-\frac{n}{2}-2} \exp\left(\frac{-n\beta_0}{2\beta}\right). \quad (16)$$

This leads to a different superstatistics, compared to the case of NO . Integrating the conditional probability $p(u|\beta)$, as in (7) but with local Maxwell-Boltzmann

distributions $p(u|\beta)$ and an inverse- χ^2 distribution $f(\beta)$, gives the marginal distribution as

$$p(u) = \sqrt{\frac{64}{\pi}} \frac{\beta_0}{\Gamma(\frac{n}{2})} \left(\frac{n\beta_0}{2}\right)^{\frac{n+1}{4}} u^{\frac{n+3}{2}} K_{\frac{1-n}{2}}\left(u\sqrt{2n\beta_0}\right) \quad (17)$$

where $K_v(z)$ is the modified Bessel function of the second order. This inverse χ^2 -superstatistical model leads to a very good description of the data, see Fig. 5.

To conclude, we have illustrated that superstatistical methods, originally introduced in nonequilibrium statistical mechanics and applied to fully developed turbulent flows and other complex systems, find new applications to model the statistics of air pollution. We find excellent agreement of simple superstatistical models with the experimentally measured pollution data. A main result is that different pollutants obey different types of superstatistics (in our case χ^2 for NO and inverse χ^2 for NO_2).

In fact, different types of local dynamics also occur (in our case locally exponential density for NO and locally Maxwell-Boltzmann for NO_2). Once the precise superstatistical model for a given pollutant has been identified, precise risk estimates of high pollution situations can be given, by integrating the tails of the probability distribution above a given threshold. These estimates could help to design tailor-made thresholds for suitable policies to tackle the pollution problem in cities. We discuss some explicit examples in the SM. The superstatistical approach presented in this Letter can easily be generalized and extended. For example we may formulate an explicit dynamical process to match the trajectories in time (in form of a superstatistical stochastic differential equation), which could lead to synthetic dynamical models and the possibility to employ short-term predictions of the pollution concentration.

We acknowledge support from EPSRC Grant No. EP/N013492/1. This project has received funding from the European Union's Horizon 2020 research and innovation programme under the Marie Skłodowska-Curie grant agreement No 840825.

* b.schaefer@qmul.ac.uk

† c.beck@qmul.ac.uk

- [1] C. Beck and E. G. D. Cohen, *Physica A: Statistical mechanics and its applications* **322**, 267 (2003).
- [2] C. Beck, E. G. D. Cohen, and H. L. Swinney, *Physical Review E* **72**, 056133 (2005).
- [3] C. Beck, *Physical Review Letters* **98**, 064502 (2007).
- [4] K. E. Daniels, C. Beck, and E. Bodenschatz, *Physica D: Nonlinear Phenomena* **193**, 208 (2004).
- [5] S. Rizzo and A. Rapisarda, in *AIP Conference Proceedings* (AIP, 2004), vol. 742, pp. 176–181.
- [6] P. Jizba and H. Kleinert, *Physical Review E* **78**, 031122 (2008).
- [7] A. V. Chechkin, F. Seno, R. Metzler, and I. M. Sokolov, *Physical Review X* **7**, 021002 (2017).
- [8] B. Schäfer, C. Beck, K. Aihara, D. Witthaut, and M. Timme, *Nature Energy* **3**, 119 (2018).
- [9] G. C. Yalcin, P. Rabassa, and C. Beck, *Journal of Physics A: Mathematical and Theoretical* **49**, 154001 (2016).
- [10] C. De Michele and F. Avanzi, *Scientific Reports* **8**, 14204 (2018).
- [11] E. D. Amster, M. Haim, J. Dubnov, and D. M. Broday, *Environmental Pollution* **186**, 20 (2014).
- [12] G. B. Hamra, F. Laden, A. J. Cohen, O. Raaschou-Nielsen, M. Brauer, and D. Loomis, *Environmental Health Perspectives* **123**, 1107 (2015).
- [13] A. S. Shah, K. K. Lee, D. A. McAllister, A. Hunter, H. Nair, W. Whiteley, J. P. Langrish, D. E. Newby, and N. L. Mills, *BMJ* **350**, h1295 (2015).
- [14] United States Environmental Protection Agency, *Nitrogen Dioxide (NO_2) Pollution*.
- [15] P. Domingos, A. M. Prado, A. Wong, C. Gehring, and J. A. Feijo, *Molecular Plant* **8**, 506 (2015).
- [16] J. Astier, I. Gross, and J. Durner, *Journal of Experimental Botany* **69**, 3401 (2017).
- [17] M. M. Musameh, C. J. Dunn, M. H. Uddin, T. D. Sutherland, and T. D. Rapson, *Biosensors and Bioelectronics* **103**, 26 (2018).
- [18] M. E. Barsan (2007).
- [19] Environmental Research Group (ERG) at King's College London, *London air*, URL <https://www.londonair.org.uk>.
- [20] C. Tsallis, *Introduction to nonextensive statistical mechanics: approaching a complex world* (Springer, 2009).
- [21] R. Hanel, S. Thurner, and M. Gell-Mann, *Proceedings of the National Academy of Sciences* **108**, 6390 (2011).
- [22] P. Jizba and J. Korb, *Physical Review Letters* **122**, 120601 (2019).
- [23] C. Beck, *Physical Review Letters* **87**, 180601 (2001).
- [24] G. W. Fuller and A. Font, *Science* **365**, 322 (2019).
- [25] Q. Di, Y. Wang, A. Zanobetti, Y. Wang, P. Koutrakis, C. Choirat, F. Dominici, and J. D. Schwartz, *New England Journal of Medicine* **376**, 2513 (2017).
- [26] World Health Organization (WHO), *How air pollution is destroying our health* (2019), URL <https://www.who.int/air-pollution/news-and-events/how-air-pollution-is-destroying-our-health>.
- [27] H. Walton, D. Dajnak, S. Beevers, M. Williams, P. Watkiss, and A. Hunt, London: Kings College London, Transport for London and the Greater London Authority (2015).
- [28] Health Effects Institute, Special Report (2018).

SUPPLEMENTAL MATERIAL

This supplemental Material provides calculations of some equalities used in the main text, such as relationships between mean, variance and kurtosis for the relevant distributions. We also display how the long time scale is determined and explicitly discuss how the knowledge of concentration probability distributions could be used to set pollution thresholds and policies.

NO

Calculation of λ_q

$$\begin{aligned} \mu = \langle u \rangle &= (2-q)\lambda_q \int_0^\infty u [1 + (q-1)\lambda_q u]^{\frac{1}{1-q}} du \\ &= \frac{(2-q)\Gamma(2)\Gamma\left(\frac{3-2q}{q-1}\right)}{\lambda_q(q-1)^2\Gamma\left(\frac{1}{q-1}\right)} \\ &= \frac{1}{\lambda_q(3-2q)} \end{aligned} \quad (18)$$

which gives

$$\lambda_q = \frac{1}{\mu(3-2q)}. \quad (19)$$

Calculation of mean μ of Exponential Distribution

$$\begin{aligned} \mu = \langle u \rangle &= \beta \int_0^\infty u \exp(-\beta u) du \\ &= \frac{1}{\beta} \end{aligned} \quad (20)$$

Calculation of kurtosis κ of Exponential Distribution

$$\begin{aligned} \kappa &= \frac{\langle (u-\mu)^4 \rangle}{\langle (u-\mu)^2 \rangle^2} = \frac{\int_0^\infty (u-\mu)^4 \beta \exp(-\beta u) du}{\left(\int_0^\infty (u-\mu)^2 \beta \exp(-\beta u) du\right)^2} \\ &= \frac{\int_0^\infty (u^4 - 4u^3\mu + 6u^2\mu^2 - 4u\mu^3 + \mu^4) \beta \exp(-\beta u) du}{\left(\int_0^\infty (u^2 - 2u\mu + \mu^2) \beta \exp(-\beta u) du\right)^2} \\ &= \frac{24 - 24\mu\beta + 12\mu^2\beta^2 - 4\mu^3\beta^3 + \mu^4\beta^4}{4 - 8\mu\beta + 8\mu^2\beta^2 - 4\mu^3\beta^3 + \mu^4\beta^4} \\ &= 9, \end{aligned} \quad (21)$$

using $\mu = \frac{1}{\beta}$.

Superstatistical calculation of q -Exponential Distribution

$$p(u|\beta) = \beta \exp(-\beta u) \quad (22)$$

$$\begin{aligned} p(u) &= \int_0^\infty p(u|\beta) f(\beta) d\beta \\ &= \frac{1}{\Gamma\left(\frac{n}{2}\right)} \left(\frac{n}{2\beta_0}\right)^{\frac{n}{2}} \int_0^\infty \beta^{\frac{n}{2}} \exp\left(-\beta\left(\frac{n}{2\beta_0} + u\right)\right) d\beta, \end{aligned} \quad (23)$$

which can be evaluated to

$$p(u) = (2-q)\lambda_q [1 + (q-1)\lambda_q u]^{\frac{1}{1-q}}, \quad (24)$$

if we identify

$$-\left(\frac{n+2}{2}\right) = \frac{1}{1-q}, \quad (25)$$

$$\frac{1}{2}(q-1)\lambda_q = \frac{\beta_0}{n}, \quad (26)$$

where β_0 is the mean of β .

Determining the long time scale T

We determine the long time scale T from the time series using Equ. (4) from the main text given as

$$\kappa(\Delta t) = \frac{1}{t_{max} - \Delta t} \int_0^{t_{max} - \Delta t} dt_0 \frac{\langle (u - \bar{u})^4 \rangle_{t_0, \Delta t}}{\langle (u - \bar{u})^2 \rangle_{t_0, \Delta t}^2}. \quad (27)$$

The long time scale T is defined as $T := \Delta t$ such that $\kappa(\Delta t) = 9$. Here, we compute the local kurtosis κ as a function of the time window Δt and thereby determine T .

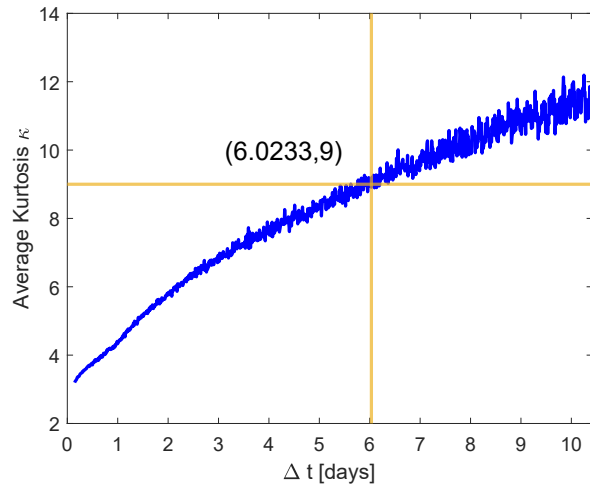


Figure 6. The average kurtosis κ as given by Eq.(4) is plotted as a function of the time window Δt (blue). The crossing between the horizontal line at $\kappa = 9$ (the kurtosis of an exponential distribution) and the κ vs. Δt curve gives the value for $\Delta t = T \approx 6$.

NO_2

Calculation of σ_q

$$\begin{aligned}
\mu = \langle u \rangle &= \frac{\sigma_q^{3/2}}{Z} \int_0^\infty u^3 [1 + (q-1)\sigma_q u^2]^{-\frac{1}{1-q}} du \\
&= \frac{\Gamma(2)\Gamma\left(\frac{3-2q}{q-1}\right)}{2Z\sigma_q^{1/2}(q-1)^2\Gamma\left(\frac{1}{q-1}\right)} \\
&= \frac{1}{2Z(2-q)(3-2q)\sigma_q^{1/2}} \\
&= \frac{2(q-1)^{3/2}\Gamma\left(\frac{1}{q-1}\right)}{\sigma_q^{1/2}\sqrt{\pi}(2-q)(3-2q)\Gamma\left(\frac{5-3q}{q-1}\right)},
\end{aligned} \tag{28}$$

which gives

$$\sigma_q = \left(\frac{2(q-1)^{3/2}\Gamma\left(\frac{1}{q-1}\right)}{\mu\sqrt{\pi}(2-q)(3-2q)\Gamma\left(\frac{5-3q}{q-1}\right)} \right)^2 \tag{29}$$

Calculation of mean μ of Maxwell-Boltzmann Distribution

$$\begin{aligned}
\mu = \langle u \rangle &= \sqrt{\frac{16}{\pi}}\beta^{3/2} \int_0^\infty u^3 \exp(-\beta u^2) du \\
&= \sqrt{\frac{16}{\pi}}\beta^{3/2} \left(\frac{\Gamma(2)}{2\beta^2} \right) \\
&= \frac{2}{\sqrt{\pi}\beta}
\end{aligned} \tag{30}$$

Calculation of kurtosis κ of Maxwell-Boltzmann Distribution

$$\begin{aligned}
\kappa &= \frac{\langle (u-\mu)^4 \rangle}{\langle (u-\mu)^2 \rangle^2} \\
&= \frac{\sqrt{\frac{16}{\pi}}\beta^{3/2} \int_0^\infty (u-\mu)^4 u^2 \exp(-\beta u^2) du}{\left(\sqrt{\frac{16}{\pi}}\beta^{3/2} \int_0^\infty (u-\mu)^2 u^2 \exp(-\beta u^2) du \right)^2} \\
&= \frac{\frac{\mu^4\sqrt{\pi}}{4\beta^{3/2}} - \frac{2\mu^3}{\beta^2} + \frac{9\mu^2\sqrt{\pi}}{4\beta^{5/2}} - \frac{4\mu}{\beta^3} + \frac{15\sqrt{\pi}}{16\beta^{7/2}}}{\sqrt{\frac{16}{\pi}}\beta^{3/2} \left(\frac{\mu^2\sqrt{\pi}}{4\beta^{3/2}} - \frac{\mu}{\beta^2} + \frac{3\sqrt{\pi}}{8\beta^{5/2}} \right)^2} \\
&= \frac{15\pi^2 + 16\pi - 192}{(3\pi - 8)^2} \approx 3.1082
\end{aligned} \tag{31}$$

Superstatistical calculation of q -Maxwell-Boltzmann Distribution

$$p(u|\beta) = \sqrt{\frac{16}{\pi}} u^2 \sigma_{mb}^{3/2} \exp(-\sigma_{mb} u^2) \tag{32}$$

$$\begin{aligned}
p(u) &= \int_0^\infty p(u|\beta) f(\beta) d\beta \\
&= \sqrt{\frac{16}{\pi}} \frac{1}{\Gamma\left(\frac{n}{2}\right)} \left(\frac{n}{2\beta_0} \right)^{\frac{n}{2}} u^2 \int_0^\infty \beta^{\frac{n+1}{2}} \exp\left(\beta \left(\frac{n}{2\beta_0} + u^2 \right)\right) d\beta,
\end{aligned} \tag{33}$$

which can be evaluated to

$$p(u) \sim u^2 \sigma_q^{3/2} [1 + (q-1)\sigma_q u^2]^{-\frac{1}{1-q}}, \tag{34}$$

if we identify

$$-\left(\frac{n+3}{2} \right) = \frac{1}{1-q}, \tag{35}$$

$$\frac{1}{2}(q-1)\sigma_q = \frac{\beta_0}{n}, \tag{36}$$

where β_0 is the mean of β .

Calculation of inverse- χ^2 superstatistical distribution based on superimposed Maxwell-Boltzmann distributions

Taking the conditional density $p(u|\beta)$ as given in (32) and the inverse- χ^2 distribution for the distribution $f(\beta)$, the probability density $p(u)$ is

$$\begin{aligned}
p(u) &= \sqrt{\frac{16}{\pi}} \frac{\beta_0}{\Gamma\left(\frac{n}{2}\right)} \left(\frac{n\beta_0}{2} \right)^{\frac{n}{2}} u^2 \int_0^\infty \beta^{-\frac{(n+1)}{2}} \exp\left(-\frac{n\beta_0}{2\beta} - \beta u^2\right) d\beta \\
&= \sqrt{\frac{64}{\pi}} \frac{\beta_0}{\Gamma\left(\frac{n}{2}\right)} \left(\frac{n\beta_0}{2} \right)^{\frac{n+1}{4}} u^{\frac{n+3}{2}} K_{\frac{1-n}{2}}\left(u\sqrt{2n\beta_0}\right)
\end{aligned} \tag{37}$$

Extra Figures

We repeat Fig. 3 from the main text for local NO_2 concentrations, i.e. analyzing brief periods of the NO_2 trajectory. Fig. 7 illustrates that in good approximation the local behavior follows Maxwell-Boltzmann distributions with fluctuating variance. Further, we also determine the long time scale T for the local Maxwell-Boltzmann distributions by setting $T := \Delta t$ for the local kurtosis $\kappa(\Delta t) \approx 3.1082$, following Eq. (4) from the main text again. See Figs. 7 and 8.

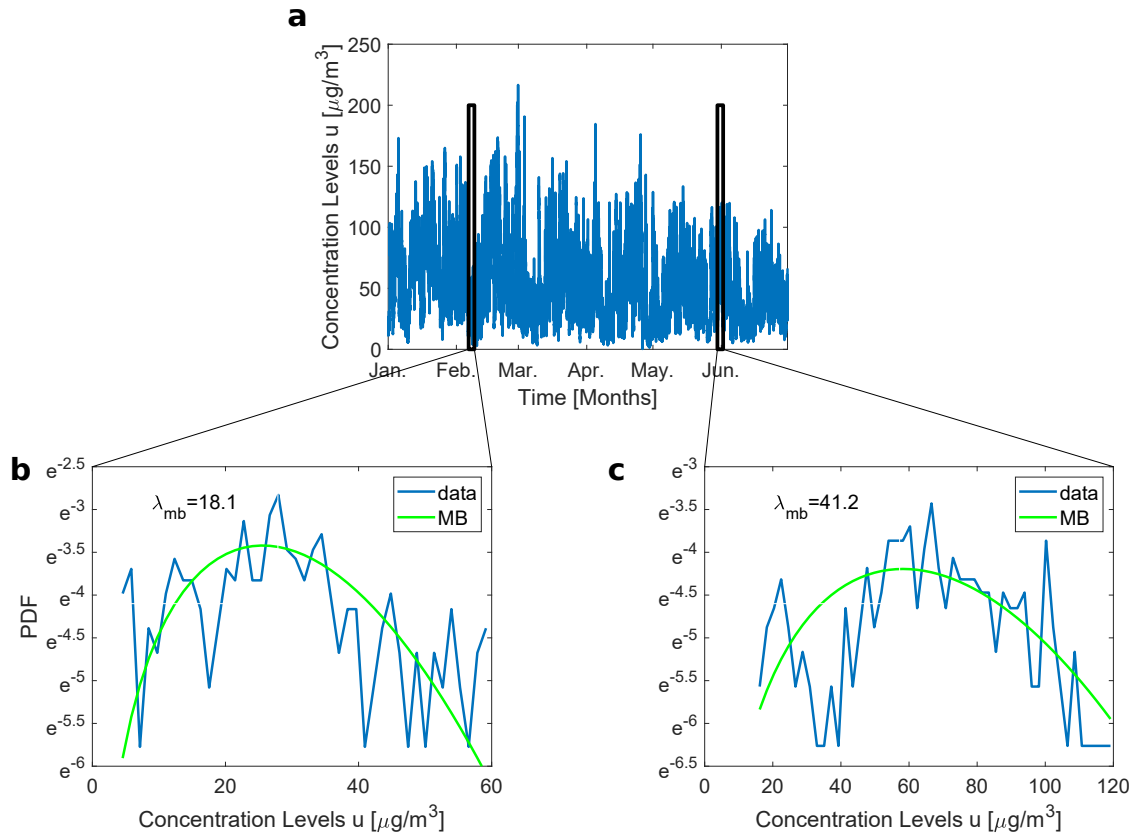


Figure 7. NO_2 concentrations locally follow Maxwell-Boltzmann distributions. a: We plot the NO_2 concentration for several months in 2010, with two periods of length $\Delta t = T \approx 2.6$ days highlighted, whose distributions are explored in panels b and c. The histograms of panels b and c are fitted with Maxwell-Boltzmann distributions and we note their respective λ_{mb} -values, which are strongly varying in time.

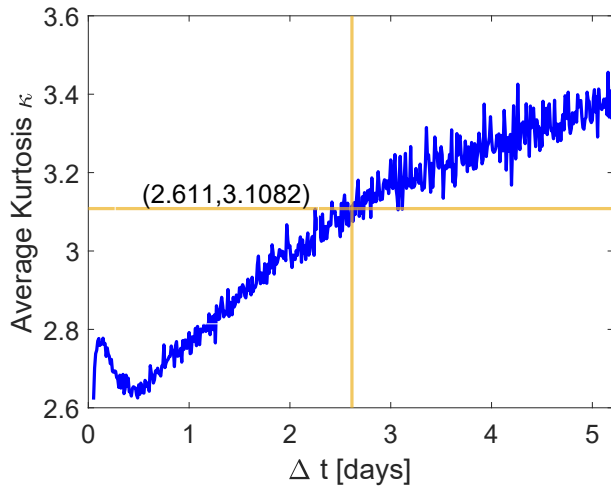


Figure 8. The average kurtosis κ is plotted as a function of the time window Δt . The crossing between the horizontal line at $\kappa = 3.1082$ (the kurtosis of a Maxwell-Boltzmann distribution) and the κ vs. Δt curve gives the value $\Delta t = T = 2.61$.

Thresholds and policies

Policies to tackle pollution in cities often focus on thresholds and compliance with these thresholds. This then often leads to pollution just below the threshold in many regions. However, in many cases it may be more reasonable to reduce the overall exposure to pollutants [24]. Weather is responsible for many fast variations of the air pollution [24]. The focus on threshold is especially dangerous as there is strong evidence that even small concentrations of pollutants, below national standards, increase the death rate [25]. The UK government (Dept. of Health & Social Care) calls air pollution a "health emergency" and the World Health Organization (WHO) judges the situation similarly on a global scale [26]. Note that about 9500 premature deaths are attributed to air pollution in London alone every year [27]. On a global scale this number rises to about 4.9 million premature deaths, making air pollution the fifth leading cause of mortality worldwide[28].

So let us finally sketch how the knowledge of the probability density function (PDF) allows estimates of threshold crossings and total exposure. Setting thresholds on

pollutant concentrations is a popular tool when setting pollution policies. Simultaneously, data coverage might not be very good in all locations. Especially if data is not available for the full time period of interest but only for a few months, estimates on how frequently thresholds are violated are difficult to obtain. As soon as we are able to determine the PDF $p(u)$ for the concentration levels u , we can easily compute the number of days where thresholds are violated as

$$N_{u>u_{\text{threshold}}} = 365 \int_{u_{\text{threshold}}}^{\infty} p(u) du. \quad (38)$$

This integral can be easily evaluated numerically, using q -exponential distributions for NO , see Eq. (8) from the main text, and Eq. (17) from the main text for NO_2 , consistent with experimental observations.

The number of threshold violations explicitly depends on the parameters λ_q and q , which have to be determined from the data sets but can then be compared between different locations and time periods. Having these two parameters explicitly disentangles two aspects: The rate of (rare) extreme events, encoded in q and the overall variability of the pollutant concentration, encoded in λ_q (or λ_{mb} for NO_2).

Complementary to thresholds, policies could instead focus on the total pollution exposure (TPE) describing the average amount citizens are exposed to. Again, this is easily computed from the PDF as

$$TPE = 365 \int_0^{\infty} p(u) u du. \quad (39)$$